JACS
JOURNAL OF THE AMERICAN CHEMICAL SOCIETY
Article
pubs.acs.org/JACS

3d−4f $\{Co^{II}_3Ln(OR)_4\}$ Cubanes as Bio-Inspired Water Oxidation Catalysts

Fabio Evangelisti, René Moré, Florian Hodel, Sandra Luber,* and Greta Ricarda Patzke*

Department of Chemistry, University of Zurich, Winterthurerstrasse 190, CH-8057 Zurich, Switzerland

Supporting Information

ABSTRACT: Although the $\{CaMn_4O_5\}$ oxygen evolving complex (OEC) of photosystem II is a major paradigm for water oxidation catalyst (WOC) development, the comprehensive translation of its key features into active molecular WOCs remains challenging. The $[Co^{II}_3Ln(hmp)_4(OAc)_5H_2O]$ ($\{Co^{II}_3Ln(OR)_4\}$; Ln = Ho−Yb, hmp = 2-(hydroxymethyl)pyridine) cubane WOC series is introduced as a new springboard to address crucial design parameters, ranging from nuclearity and redox-inactive promoters to operational stability and ligand exchange properties. The $\{Co^{II}_3Ln(OR)_4\}$ cubanes promote bioinspired WOC design by newly combining Ln^{3+} centers as redox-inactive Ca^{2+} analogues with flexible aqua-/acetate ligands into active and stable WOCs (max. TON/TOF values of 211/9 s^{-1}). Furthermore, they open up the important family of 3d−4f complexes for photocatalytic applications. The stability of the $\{Co^{II}_3Ln(OR)_4\}$ WOCs under photocatalytic conditions is demonstrated with a comprehensive analytical strategy including trace metal analyses and solution-based X-ray absorption spectroscopy (XAS) investigations. The productive influence of the Ln^{3+} centers is linked to favorable ligand mobility, and the experimental trends are substantiated with Born−Oppenheimer molecular dynamics studies.

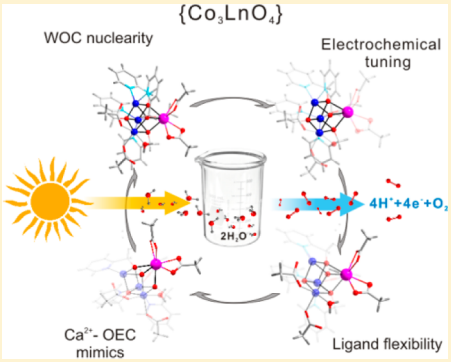

1. INTRODUCTION

Artificial photosynthesis is a sustainable concept for the direct conversion of solar resources into storable chemical fuels.[1] To date, the targeted development of efficient water oxidation catalysts (WOCs) remains a synthetic and analytical challenge.[2] The cuboidal $\{CaMn_4O_5\}$ oxygen evolving complex (OEC) of nature's photosystem II (PSII) is a leading WOC design paradigm,[3] while its structure and mechanisms still remain under intense investigation. The current discrepancy between elaborate synthetic OEC models on the one hand, and their lack of catalytic activity on the other calls for further explorations of cubane-type WOCs.[4] In view of the limited number of such examples (Table 1), there is plenty of room to promote the translation of OEC features into molecular catalysts.[5]

The $[Co^{II}_3Ln(hmp)_4(OAc)_5H_2O]$ ($\{Co^{II}_3Ln(OR)_4\}$; Ln = Ho−Yb, hmp =2-(hydroxymethyl)pyridine) WOC series advances bioinspired catalyst design through the combination of unprecedentedly close OEC analogies with active and stable water oxidation performance (Figure 1). Moreover, the $\{Co^{II}_3Ln(OR)_4\}$ cubanes are the first 3d−4f complexes to catalyze key photochemical processes, thereby opening up this compound family for homogeneous catalysis.[6]

Generally, the gap between the rapidly growing family of Co-based and other transition metal WOCs[7] and their underlying mechanisms and structure−activity relationships is widening.[8] The title compounds serve as excellent model systems to further investigate crucial trends and mechanisms in OEC-inspired WOC design.[9]

1.1. Co vs Mn Centers in Biorelated Molecular WOCs.

Co-cubane WOCs are now about to be explored, especially as closer OEC analogues,[10] while the WOC activity of a stable tetranuclear Mn-WOC has only been reported for a single $\{Mn_4\}$-polyoxometalate to date.[11]

Although impressive synthetic progress was made on $\{CaMn_3O_4\}$-derived cores and PSII-related cubanes,[12] Mn-cubanes hitherto turned out to be unstable under catalytic conditions.[12c] In contrast, electrochemical studies on various $\{Mn_3MO_n\}$ cubanes strongly suggested catalytic optimization strategies based on the introduction of redox-inert cations as Ca^{2+}-OEC analogues.[12c,13] Given this lack of WOC activity among Mn-based cubane complexes, we here selected Co-containing cubanes to newly implement this concept for mechanistic follow-up studies.

1.2. Stable Co-Cubanes for Mechanistic Studies.

Recent investigations on $\{Co^{III}_4O_4\}$ cubane WOCs[5b,c] and Co-POM catalysts[14] have raised the demand for stable target compounds for structure−activity relationship studies. We present a widely applicable strategy to prove the identity of polynuclear WOCs as true active homogeneous species. Stability and integrity of the $\{Co^{II}_3Ln(OR)_4\}$ WOCs is confirmed with a newly designed analytical workflow encompassing a wide range of methods to exclude metal leaching or decomposition processes and secondary catalyst formation.

Received: June 5, 2015
Published: August 12, 2015

DOI: 10.1021/jacs.5b05831
J. Am. Chem. Soc. 2015, 137, 11076−11084

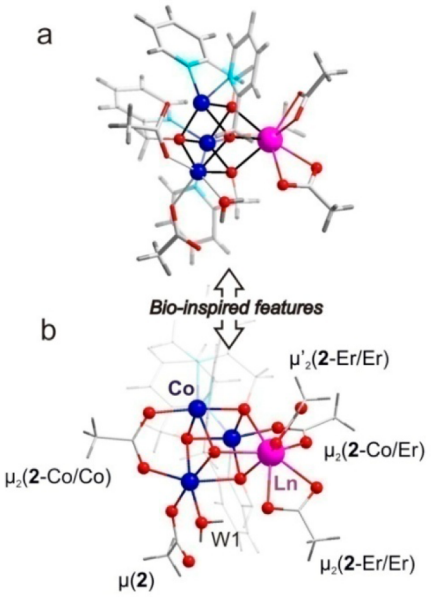

Figure 1. Structural motif of 2-Ln cubanes: (a) Representative crystal structure (Co: blue; Ln: pink; O: red; C: white; H: gray); (b) bioinspired $\{Co^{II}_3Ln\}$ core and ligand environment of aqua ligand (W) and mono (μ) as well as bidentate acetate (μ_2) ligands.

1.3. From OEC Features to Molecular WOC Design. The versatile new $\{Co^{II}_3Ln(OR)_4\}$ systems are the first WOC-active Co-cubanes containing Ln^{3+} cations as Ca^{2+}-mimics (Figure 1b). Comparison to our recently introduced all-Co $\{Co^{II}_4(OR)_4\}$ cubane[10d] covers four key design issues: (a) transition metal core nuclearity, (b) OEC-inspired ligand flexibility vs water oxidation activity,[15] along with redox-inert Ln^{3+} cations as (c) electrochemical tuning agents, and (d) biorelated promoters mimicking the Ca^{2+} site of the OEC.[12a] In addition, the title compounds offer fine-tuned magnetic properties.[16]

As for core nuclearity, the essential role ascribed to tetranuclear Co-WOCs[2b,5a,8c] stands in contrast to mono-[17,18] or polynuclear[19,20] Co-based photo- and electrocatalysts. Theoretical studies furthermore associated the remarkable activity of CoPi electrocatalysts[21] with only one or two active cobalt sites.[22] Modeling[8d,23] and catalytic[10c] studies on $\{Co_4O_4\}$-type WOCs outline the importance of mobile aqua ligands for efficient O_2 evolution.

In the following, we establish operational stability of the $\{Co^{II}_3Ln(OR)_4\}$ series under homogeneous photocatalytic conditions with a wide spectrum of complementary techniques. We demonstrate the productive effect of bioinspired Ln^{3+} centers[24] on the photochemical WOC performance and the ligand mobility of Co-cubanes, and we substantiate our experimental results with modeling studies.

2. RESULTS AND DISCUSSION

2.1. Structure and Characterization. The isostructural 2-Ln series of $[Co^{II}_3Ln(hmp)_4(OAc)_5H_2O]$ (Ln = Ho, Er, Tm, Yb) cubanes and the reference WOC $[Co^{II}_4(hmp)_4(\mu\text{-}OAc)_2(\mu_2\text{-}OAc)_2(H_2O)_2]$ **1** (cf. Scheme S1) were obtained from a modified protocol of Wang et al.[16] and our own work.[10d] The solid state phase purity of all the recrystallized samples was confirmed with a wide range of methods (e.g., PXRD, HR-ESI-MS, and FT-IR data in Figures S1–S5), along with stability tests in solution (e.g., UV–vis spectra and monitoring in Figures S6, S25). The tetrametallic $\{Co^{II}_4(OR)_4\}$ and $\{Co^{II}_3Ln(OR)_4\}$ cores display different distribution patterns of the same ligand set, whereas **1** contains four monodentate ligands (two acetate and water molecules, respectively), and a chelating acetate ligand replaces one of the water molecules in the 2-Ln cubanes. The pK_a of the aqua ligand decreases slightly over the series [8.9 (2-Er) to 8.5 (2-Yb), cf. Figure S7 and Table S2].

2.2. WOC Performance. The WOC performance of the 2-Ln cubane series was monitored vs **1** with complementary standard techniques in the presence of $[Ru(bpy)_3]^{2+}$ as a photosensitizer (PS) and $S_2O_8^{2-}$ as an electron acceptor (EA) (Figure 2, see SI for details).[25] The overall oxygen amount

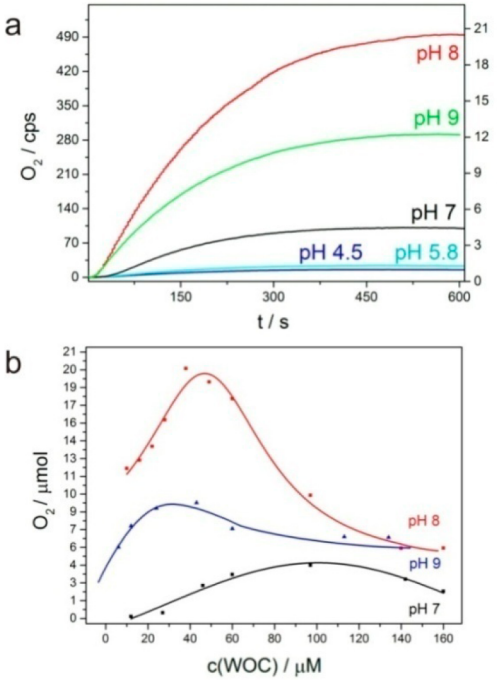

Figure 2. WOC performance of the 2-Ln (Ln = Ho–Yb) cubane series. (a) Visible-light-driven WOC activity of 2-Er (representative example) at pH 4.5, 5.8, 7, 8, and 9; (b) concentration-dependent photochemical O_2 evolution for 2-Er under standard conditions (1 mM $[Ru(bpy)_3]^{2+}$, 5 mM $Na_2S_2O_8$, 470 nm) at pH 7 (black), pH 8 (red), and pH 9 (blue) for different catalyst concentrations (cf. Table S3).

produced during catalysis and the duration of the catalytic process are both limited by the amount of electron acceptor used. Control experiments under optimized conditions proved unambiguously that oxygen evolution only occurs in the simultaneous presence of all three key components, i.e., PS, EA, and cubane cluster (Table S7). The possibility of Co^{2+} leaching from the molecular WOCs was evaluated with further reference tests in the corresponding pH and concentration range (Table S8 and Figures S18–S20, cf. section on WOC stability tests below). pH-dependent WOC performance among the 2-Ln series (Table S3) peaked around 8–9 concerning the overall oxygen yield, turnover number (TON), and turnover frequency (TOF). TON and TOF values for **1** and 2-Ln display different concentration dependencies (Figure 2b and Figures S8–S13, Tables S4–S5)[10d] with maximum TON values of 211 and 163 for 2-Er and 2-Ho, respectively (pH 8, 10 μM). These WOCs also display the highest TOF values among the series at pH 9 with 9.6 s^{-1} (2-Ho, 12 μM) and 8.9 s^{-1} (2-Er, 33 μM; full data set: Tables S4–S5). The entire 2-Ln WOC series exhibits pseudo first-order oxygen evolution kinetics with respect to the WOC

DOI: 10.1021/jacs.5b05831
J. Am. Chem. Soc. 2015, 137, 11076–11084

concentration and comparable rate constant values (0.55−0.59 μmol s^{-1} from 2-Ho to 2-Yb, cf. Figure S11) over the 5−50 μM concentration range.

Higher 2-Ln concentrations (50−250 μM) change the reaction kinetics and reduce the WOC performance. In contrast, **1** follows pseudo-first-order kinetics throughout the 10−200 μM range. Peak TOF values and O_2 yields at pH 8 and 9, respectively, for both **1** and the 2-Ln series (Figure 2) indicate a correlation between aqua ligand deprotonation and optimal WOC activity. Most importantly, the 2-Ln WOCs clearly outperform **1** at lower concentrations (5−30 μM for 2-Ln vs 60−100 μM for **1**) in maximum TON (211 vs 40) and TOF (9.6 vs 7.0 s^{-1}, cf. Figure 2b and Figure S8) values. Reference experiments with Co^{3+}/Ln^{3+}/hmp solutions in various permutations furthermore showed that the embedment of the Ln^{3+} centers into the active cubane WOC architecture is essential for the observed performance enhancement (Figure S19). The 2-Er and 2-Ho representatives rank among leading Co-containing molecular WOCs to date (Tables 1 and S10), and they display the highest WOC activity in borate buffer media (Table S3).

Table 1. Comparison of 1, 2-Ln, and Reference Co-WOCs: TON/TOF and Rate Constants for Hole Scavenging (k_{hs})

Co-WOC	TON/TOF[a]	k_{hs}[d] (10^6 M s^{-1})
$[Co_3Ln(hmp)_4(OAc)_5H_2O]$ (Ln = Ho, Er, Tm, Yb)[b] [this work]	160−220/9 s^{-1}	0.70 ± 0.04, 0.37 ± 0.05, 1.9 ± 0.4
$[Co^{II}_4(hmp)_4(\mu\text{-}OAc)_2(\mu_2\text{-}OAc)_2(H_2O)_2]$[b,10d]	40/5 s^{-1}	11 ± 3, 5 ± 1, 6 ± 1
$[Co^{III}_4O_4(OAc)_4(py)_4]$[c,10a]	40/2 × 10^{-2} s^{-1}	12 ± 4, 16 ± 4, --
$[Co^{III}_4O_4(OAc)_4(p\text{-}C_5H_4X)_4]$ (X = H, Me, *t*-Bu, OMe, Br, COOMe, CN)[c,10b]	140[e]/ 7 × 10^{-2} s^{-1}[e]	--, 250[e], --
Co(II)Slp (slp = *N*,*N*′-bis(salicylaldehyde)-1,2-phenylenediamine)[b,17]	17/5 × 10^{-3} s^{-1}	112, --, --

[a]TOFs were determined by different methods and are not further compared below. [b](H_2O, PS = $[Ru(bpy)_3]^{2+}$/ EA = $S_2O_8^{2-}$). [c](H_2O/CH_3CN; PS = $[Ru(bpy)_3]^{2+}$/ EA = $S_2O_8^{2-}$). [d]Aqueous solution at pH 7, 8 and 9, respectively, if not otherwise specified. [e]Maximum values for 50:50 (H_2O/CH_3CN) solution at pH 8 (X = OMe).

2.3. Operando Electrochemical WOC Properties. Electrochemical characterizations of the 2-Ln WOC series in operando buffer media (representative data at pH 8 for 2-Er cf. Figure S15) display the reversible Co^{II}/Co^{III} redox couple around $E_{1/2}$ = 0.88 V (vs Ag/AgCl) over the entire Ho−Yb series, followed by the onset of the catalytic wave around 1.1 V (vs Ag/AgCl) in line with the thermodynamic requirements for hole transfer from the PS (Figure S15). The pH-dependent linear decrease of the Co^{II}/Co^{III} redox potential (49 mV/pH from pH 4 to 11) (Figure S14) clearly points to a proton-coupled electron transfer process, and the spectrophotochemically determined pK_a value agrees well with the Pourbaix diagram (Figure S14). The higher average value for the 2-Ln series (0.88 V at pH 8) compared to **1** (0.55 V vs Ag/AgCl) indicates a significant effect of the lanthanide ions on the redox potential (ligand effects were excluded). All of the Ln^{3+} ions raise the onset potential of the catalytic wave of 2-Ln in aqueous media by approximately 0.15 V in comparison to **1** (Figure S15).

Interestingly, the Co^{II}/Co^{III} redox potential of the entire $\{Co^{II}_3XO_4\}$ cubane WOC series can be also fine-tuned in nonaqueous media as a function of the metal center X (full data set for **1** and 2-Ln in CH_2Cl_2/$TBAPF_6$ in Figure 3a) over the

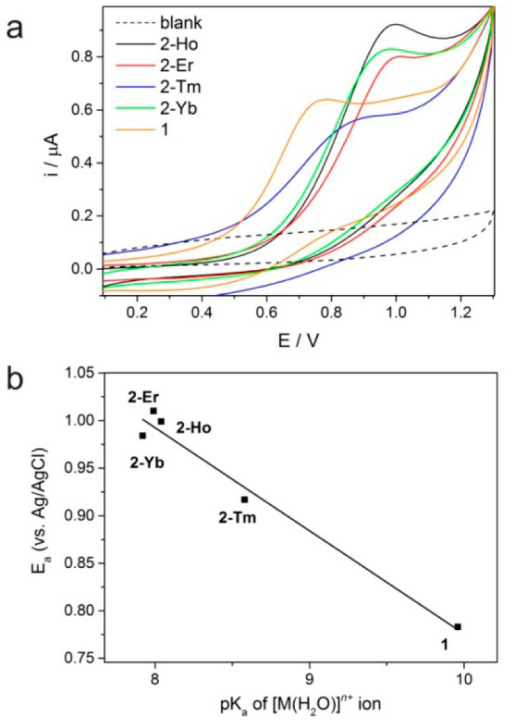

Figure 3. (a) Cyclic voltammograms of 100 μM **1** and of the 2-Ln (Ln = Ho, Er, Tm, Yb) series in 0.1 M $TBAPF_6$/CH_2Cl_2. Scan rate: 100 mV/s; GC working electrode, Ag/AgCl reference electrode, and Pt wire counter electrode. (b) Oxidation potential of the 2-Ln series (0.1 M $TBAPF_6$/CH_2Cl_2) vs pK_a of the corresponding $[M(H_2O)_x]^{n+}$ ion as a parameter for the Lewis acidity.

range from 0.78 V (X = Co^{II}) to 0.98 V (X = Yb^{III}). The absence of the corresponding reduction peak might indicate aqua/acetate ligand exchange processes in line with mechanistic studies and calculations (cf. below). In agreement with the trends for aqueous media, the Ln^{3+} ions raise the Co^{II}/Co^{III} redox potential by approximately 0.12 V (Tm^{III}) and ∼0.2 V (Ho^{III}, Er^{III}, Yb^{III}) compared to **1** in organic solvents. Furthermore, the redox potential in nonaqueous media increases linearly with the Lewis acidity of the Co^{2+} and Ln^{3+} centers from **1** to the 2-Ln series with ca. 0.1 V per pK_a unit (Figure 3b and Table S6).[12a] The $\{Co^{II}_3Ln(OR)_4\}$ cubanes are the first photochemical WOCs implementing the recent trend toward redox potential modulation by redox-inactive centers.[4a,9a,12a]

Stability under electrochemical conditions was established with bulk electrolysis of 2-Er and reference Co^{2+} solutions performed at 1 V (Figure S16). The results clearly showed different current density profiles of Co^{2+} and 2-Er. Post-electrolytic SEM/EDX investigations of the electrode surfaces furthermore displayed different surface morphologies and EDX spectra of the deposits resulting from 2-Er and Co^{2+}, respectively (Figure S17). However, stability of the 2-Ln family under $[Ru(bpy)_3]^{2+}$/$S_2O_8^{2-}$ assay conditions is more relevant for the present study, as discussed below.

2.4. Strategy for WOC Stability Tests. In light of recent investigations into the active species associated with $\{Co^{III}_4O_4\}$ cubane WOCs,[5b] the operational stability of the title compounds was tested on different levels (Figure 4). We created a systematic analytical workflow:[26−28] (I) exclusion of secondary heterogeneous (nano-)WOCs; (II) trace metal analyses; (III) structural integrity of the cluster core under catalytic conditions.

DOI: 10.1021/jacs.5b05831
J. Am. Chem. Soc. 2015, 137, 11076−11084

I. Basic stability tests and exclusion of nanoparticles
Step a (*WOC tests*), Step b (*Co^{2+}-tests*),
Step c (*Photosensitizer and persulfate recyclings*), Step d (*DLS tests*)

II. Trace metal analyses
(a) Exclusion of Co leaching with complexing agents
(b) Exclusion of Co-nanocatalysts with ICP-MS analyses

III. Structural integrity of the 2-Ln WOCs
(a) Spectroscopic tests, (b) HPLC analyses, (c) EXAFS/XANES solution phase tests, (d) Mass spectroscopic analyses

Figure 4. Overall workflow and strategy for WOC stability tests.

2.4.1. Basic Stability Tests and Exclusion of Nanoparticles. First, oxygen evolution with the 2-Ln WOC series requires the presence of all system components (Table S7); i.e., $\{Co^{II}_3Ln(OR)_4\}$ cubane catalysts are a prerequisite. Next, secondary $CoO_x/Co(OH)_2$ nanoparticles as a possible consequence of hypothetical Co^{2+} leaching were ruled out in four steps: (a) kinetic analyses (Figures S18–S22), (b) WOC efficiency comparisons under standardized conditions, (c) comparative recycling tests (Figures S23, S24, and Table S9), and (d) dynamic light scattering (DLS) investigation of postcatalytic solutions (Figures S25–26).

2.4.1.1. Step a. Clark electrode monitoring of 2-Ln WOCs vs Co^{2+} reference solutions (Figure S18–S21) clearly shows that oxygen evolution starts almost immediately with 2-Ln, while Co^{2+} solutions display an average induction time of 30 s in agreement with our previous investigation of compound **1**.[10d]

2.4.1.2. Step b. The cubane WOCs outperform secondary CoO_x species in representative comparisons (2-Ho vs equimolar Co^{2+} solutions, Figure S22). It is noteworthy, however, that catalytic optimization strategies are not the main focus of the present study. In the first place, we introduce a stable molecular cubane catalyst family for systematic structure–activity relationship (SAR) and modeling studies of bioinspired WOCs (cf. Figures S18–22).

2.4.1.3. Step c. Recycling tests were conducted with two different setups: *persulfate-type* (EA replenished) and *photosensitizer-type* runs (addition of new PS or PS/EA). Peak WOC activity and persulfate-type recycling behavior of the stable molecular catalysts compare favorably with the reference $CoO_x/Co(OH)_2$ samples formed in situ. The cubane-type WOCs sustain two recycling runs with fresh $Na_2S_2O_8$ and readjustment of the pH value (Figure S23 and Table S9), while lower performance after the third cycle is mainly ascribed to PS decomposition and accumulation of side products. However, the lower 2-Ln activity in photosensitizer-type tests differed clearly from in situ formed $CoO_x/Co(OH)_2$ reference species under the same recycling conditions (Figure S24).

2.4.1.4. Step d. Most importantly, DLS results for pre- and postcatalytic 2-Ln reaction mixtures (Figure S25, top) do not display significant differences from the mQH_2O reference. Consequently, CoO_x or any other nanoparticles are absent before and after the photocatalytic process. The 2-Ln cubanes even retain their catalytic activity after 3 weeks of aging without formation of nanoparticles (Figure S21). In sharp contrast, Co^{2+} reference solutions immediately form large nano- and microscale particles (Figure S25, bottom) before irradiation, which persist in the postcatalytic mixtures.

2.4.2. Trace Metal Analyses. Trace metal analyses were subsequently performed to exclude hypothetical Co^{2+} leaching processes.

2.4.2.1. Exclusion of Co Leaching with Complexing Agents. First, photocatalytic WOC tests of both 2-Ln cubanes and Co^{2+} reference solutions were performed under standard conditions in the presence of increasing EDTA contents as a powerful chelating agent to check for possible Co^{2+} species. Control experiments showed that addition of EDTA before or immediately after the onset of irradiation does not influence the observed WOC performance. Most importantly, the addition of increasing EDTA does not affect the performance of 2-Er (representative for the 2-Ln series in the following), and only a very slight reduction is observed when the EDTA is extremely raised to the level of $[Ru(bpy)_3]Cl_2$–$Na_2S_2O_8$ concentrations (Figures S26). In sharp contrast, Co^{2+}-WOC activity is reduced to zero at an EDTA concentration that is well-tolerated by the cubanes (Figure S26); i.e., Co-EDTA complexes are inactive in photocatalytic water oxidation. This clearly proves that leached Co^{2+} species do not play a significant role in the WOC activity of the 2-Ln cubanes. They display unchanged performance up to a 6-fold molar excess of EDTA and are thus inert toward ligand blocking of the Co-sites. These results were confirmed using Chelex resins as a well-known chelator with special purification activity against transition metal cations. Likewise, the time scale of resin addition (before or directly during irradiation onset) did not influence the oxygen evolution results. As observed for the

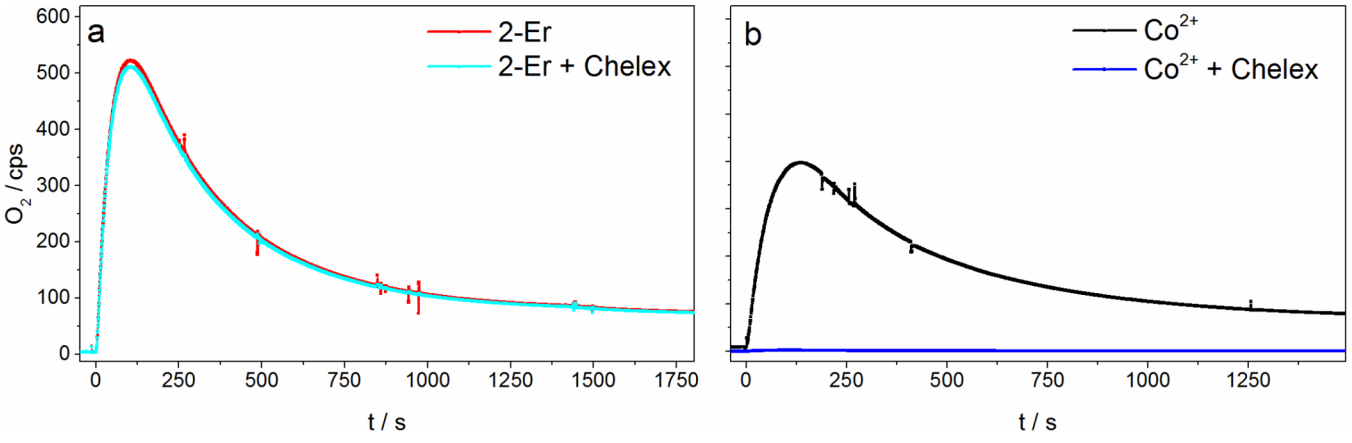

Figure 5. WOC stability tests with chelating agents: Clark-electrode kinetics of visible-light-driven O_2 evolution for 2-Er (a) and Co^{2+} (b) in the absence and presence of 20 mg of Chelex resin (for details cf. SI; conditions: 60 μM 2-Er and 3 × 60 μM Co^{2+}, 470 nm LED, 1 mM $[Ru(bpy)_3]Cl_2$, 5 mM $Na_2S_2O_8$, pH 8 borate buffer).

DOI: 10.1021/jacs.5b05831
J. Am. Chem. Soc. 2015, 137, 11076–11084

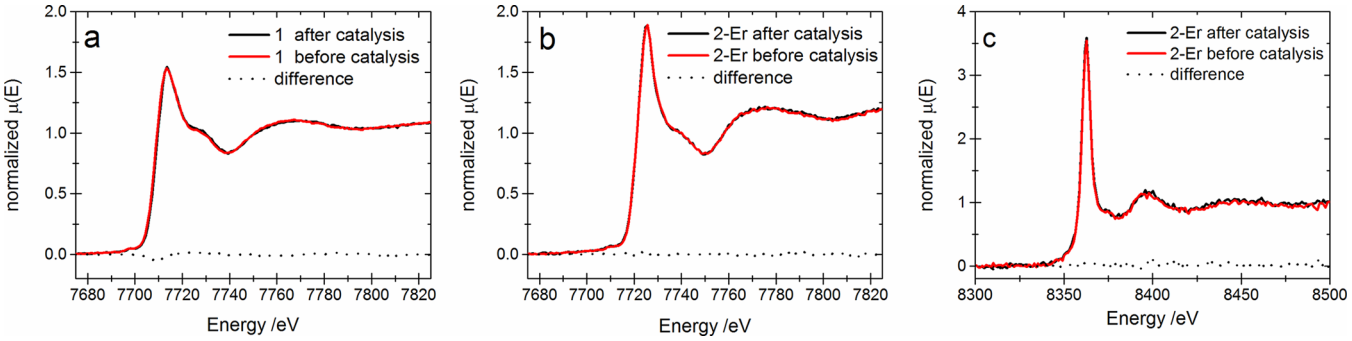

Figure 6. WOC stability tests in catalytic media: Co−K-edge XANES region of (a) **1** and (b) 2-Er before and after photocatalysis, and (c) Er L_3-edge XANES region of 2-Er before and after photocatalysis.

above EDTA assay, treatment of 2-Er with Chelex did not change the WOC activity (cf. selected concentration in Figure 5a). Reference experiments with Co^{2+} solutions (Figure 5b) demonstrate that the applied Chelex addition quantitatively removes all free cobalt ion species in solution, thereby reducing the WOC performance basically to zero. Chelex tests clearly corroborate that Co^{2+} leaching from the cubane clusters can be excluded.

2.4.2.2. Exclusion of Co-Nanocatalysts with ICP-MS Analyses. After lyophilization of a representative postcatalytic mixture of 2-Er, all components soluble in the organic phase (2-Er and $[Ru(bpy)_3]Cl_2$) were separated from possible nanoparticles and other insoluble products (mainly buffer and sulfate salts) by multiple extraction runs with methanol, followed by high-speed centrifugation (>10 000 rpm) after repeated extractions. ICP-MS checks of the combined insoluble residues for traces of cobalt or lanthanide ions gave negative results as further strong evidence for stability of the 2-Ln WOCs against decomposition under operational conditions. Furthermore, ICP-MS measurements confirmed a Co/Ln ratio of 3:1 in the organic phase, indicating the absence of possible Co-containing fragments soluble in methanol (best solvent for HR-ESI-MS investigations of the cubanes[10d]). Comparable analytical results after repetition of the above protocol in CH_2Cl_2 clearly support the presence of intact clusters in the organic phase without fragmentation or leaching.

2.4.3. Structural Integrity of the 2-Ln WOCs. The structural integrity of the 2-Ln WOCs under operational conditions was established in four steps.

2.4.3.1. Spectroscopic Tests. UV−vis aging tests in solution demonstrated that the characteristic cobalt absorptions remained constant over a period of 36 h (Figure S27). This strongly suggests stability of the 2-Ln cubanes in aqueous media. Likewise, FT-IR spectra of lyophilized aged cubane solutions are identical with those of the pristine complexes (Figure S28). Note that the reduced intensity of the UV−vis absorption bands of postcatalytic solutions is due to PS decomposition, because the d−d-transitions of the cubane complexes are generally an order of magnitude lower in intensity (cf. Figure S29).[10d]

2.4.3.2. HPLC Analyses. HPLC analyses of pre- and postcatalytic WOC solutions demonstrate that both pristine pre- and postcatalytic 2-Er cubanes are detected as virtually identical single peaks with a retention time (RT) of 18 min (Figure S30). Reference measurements with permutations of key components show that $[Ru(bpy)_3]^{2+}$ appears unambiguously as a double peak with a RT of 12 min and that a mere Co^{2+}/Ln^{3+}/hmp mixture does not give rise to cubane formation (Figure S30). This is in line with reference WOC tests (Figure S19) and permits the clear identification of intact 2-Er in the complete postcatalytic solution (Figure S30) as further proof of stability of the cubane WOCs under operational conditions.

2.4.3.3. Extended X-ray Absorption Fine Structure (EXAFS) and X-ray Absorption near-Edge Structure (XANES) Solution Phase Tests. These tests confirmed stability of the $\{Co^{II}_4(OR)_4\}$ and $\{Co^{II}_3Ln(OR)_4\}$ cubane core types under catalytic conditions. Data sets for **1** recorded in the presence of PS, electron acceptor, and borate buffer did not indicate postcatalytic changes in the oxidation state or substantial alterations in the first coordination shell of the Co^{2+} centers (cf. experimental section in the SI, Figure 6 and Figures S31−32). Likewise, Er L_3 and Co K edge XANES/EXAFS spectra of 2-Er did neither display major alterations around the Er^{3+} centers after photocatalysis (Figures 6c, S31 and Table S11), nor changes in the local Co^{2+} geometries (Figure 6a,b). XAS data in their entirety thus point to the presence of stable $\{Co^{II}_4(OR)_4\}$ and $\{Co^{II}_3Ln(OR)_4\}$ core motifs in catalytic media.

2.4.3.4. HR-ESI-MS Analyses. HR-ESI-MS analyses were furthermore applied to check for structural integrity of the 2-Ln series. Intact 2-Yb clusters (representative example for the series, cf. Figure S5 and Figure S31) were observed from aged buffered solutions with catalytic cluster concentrations after lyophilization and redissolution in methanol. However, HR-ESI-MS detection of 2-Ln in corresponding samples in the presence of catalytically relevant $[Ru(bpy)_3]^{2+}$ amounts was not possible, because the high photosensitizer concentration interfered with the detection limits (Figure S33). Cluster signals in catalytic media were only observed after 30-fold spiking above the standard value, and PS-free media were required to detect the WOC at operational concentrations (Figure S33). Selective chemical sequestration of the cluster and subsequent HR-ESI-MS detection procedures are under development.

The 2-Ln WOCs clearly passed all tests under operational conditions, setting the stage for mechanistic and computational studies.

2.5. Mechanistic Studies. Water as the main source of photocatalytic oxygen evolution was verified through good agreement of observed and expected statistical isotope ratios for both **1** and 2-Er in isotope labeling experiments using 10% $H_2{}^{18}O$ as reaction medium (for details cf. SI and Figures S34−35). Evaluation of the $m/z = 32$, $m/z = 34$ and $m/z = 36$ ratios of both **1** and 2-Er WOCs are consistent with unique incorporation of ^{18}O into O_2 from labeled water.

FT-IR monitoring of D_2O exchange experiments (Figures 7 and S37) with **1** and 2-Er in CD_3CN demonstrate near-quantitative H_2O/D_2O exchange at 15% D_2O for both cubanes.[29] Note that water exchange and release of acetate

DOI: 10.1021/jacs.5b05831
J. Am. Chem. Soc. 2015, 137, 11076−11084

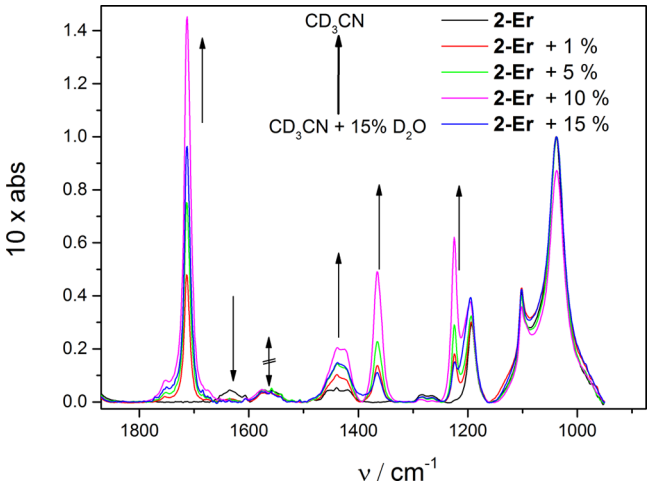

Figure 7. FT-IR spectra of 2-Er (5 mM) in CD_3CN and CD_3CN/D_2O mixtures with 1, 3, 5, 10, and 15% (v/v) D_2O (arrows indicate the increase/decrease of characteristic water and acetate vibration intensities with D_2O content; double-headed arrow = constant intensity).

ligands sets in more rapidly for the 2-Ln series at 1% D_2O, whereas **1** requires significantly higher D_2O concentrations (Figures S36, S38 and Table S12). These results agree well with computational studies on ligand exchange properties of the cubanes (cf. section below), which emerge as key characteristic performance parameter for this WOC family.

Hole scavenging kinetics for the first step of the four-electron cycle were derived from bleaching of the ground state metal-to-ligand charge transfer transition of $[Ru(bpy)_3]^{2+}$, keeping in mind that secondary oxidation processes via SO_4^- radical anions associated with ion pair effects cannot be detected. The rate constants for the first electron transfer steps with **1** and 2-Er correlate with their respective thermodynamic driving forces (Figure S15 and Table S13) as shown in previous studies on $\{Co^{III}_4(OR)_4\}$ cubanes reporting on an increase of photoinduced electron transfer with ΔE (sensitizer/catalyst).[10b] However, comparison of hole scavenging rates for **1**, 2-Er, and representative Co-WOCs (Figures S39–S43, Tables 1 and S13) indicates that high TON/TOF values are not necessarily correlated with high initial hole transfer rates.[17]

This suggests that the rate-determining step is not primary electron transfer but occurs at a later stage. Recent studies have furthermore emphasized that the turnover limiting steps of photochemical water reduction and electrochemical hydrogen evolution may differ significantly among structurally related catalysts,[30,31] so that photochemical performance cannot generally be extrapolated from electrochemical activity trends either.

2.6. Density Functional Theory-Based Calculations. Average (electronic) energies of fully solvated systems containing **1** or 2-Er (with 190–328 H_2O molecules) (Figure S47 for **1**) along with modified versions thereof were calculated from sampling at ambient conditions via Born–Oppenheimer molecular dynamics (MD) using Kohn–Sham density functional theory (DFT) (for a detailed description of the computational setup cf. SI section VI). Next, we calculated from these averages electronic energy differences for various ligand dissociations. This strategy was preferred over a static approach mainly due to a large observed dependence of energy differences on the type of solvation model and starting structure employed in DFT geometry optimizations (details cf. SI and Table S20 for thermochemical properties within a static approach). For the sake of completeness, results from "static" approaches based on geometry optimizations using the COSMO[32] solvent continuum model and for some systems with the first solvation shell explicitly represented can be found in SI section VI. Finally, we also calculated thermochemical contributions to the Gibbs energies (Table S20). For the ligand exchange reaction of **1**, these energy contributions amounted to a mere 0.16 kcal mol^{-1}. We assumed the value for the other systems to be in the same range and therefore considered the neglect of said entropic and enthalpic contributions to the energy differences justified. The electronic energies for the removal of nonbridging ligands were obtained by comparing the systems with acetate attached and OH^- at a certain distance from the cubane to the corresponding ones with OH^- attached and instead acetate in solution.

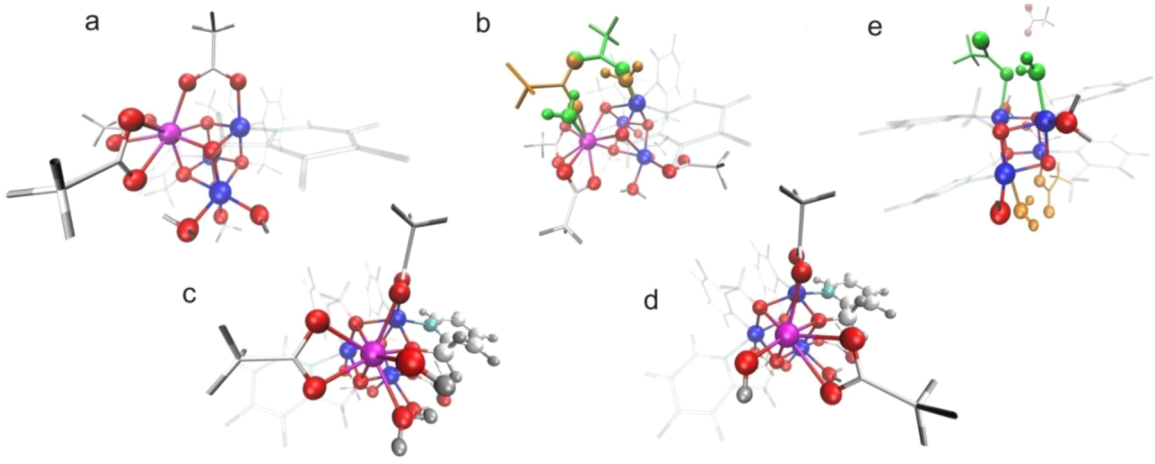

Figure 8. MD scenarios for the dissociation of acetate ligands: (a) Replacement of the monodentate μ(**2**) acetate ligand of 2-Er by HO^-; (b) both detachment options for the bridging μ_2(**2**-Co/Er)-acetate ligand from Co^{2+} (brown) or from Er^{3+} (green), followed by water association; (c) removal of the bidentate μ_2(**2**-Er/Er)-ligand along with replacement by HO^- and water association; (d) replacement of the other chelating μ'_2(**2**-Er/Er)-acetate by HO^- without association of water due to steric hindrance by the remaining μ_2(**2**-Er/Er)-ligand and the adjacent hmp; (e) partial detachment of the μ'_2(**1**) (green) and μ'_2(**1**) (brown) bridging acetate ligands from **1** after substitution of the monodentate μ(**1**) acetate ligand by HO^-.

DOI: 10.1021/jacs.5b05831
J. Am. Chem. Soc. 2015, 137, 11076–11084

In order to investigate the partial removal of bridging acetate ligands, we turned them away from one of the metal atoms they were bound to, placed a water molecule at the now vacant coordination site and ran MD. Removal of the monodentate $\mu(2)$ acetate ligand of 2-Er (cf. Figure 1 for ligand nomenclature, Figure 8a, Table S15 and Figure S48), followed by HO^- substitution at the Co^{2+} center, is energetically favorable by approximately −54 kcal mol^{-1}. In comparison, loss of the chelating μ_2(2-Er/Er)- and μ'_2(2-Er/Er)-acetate ligands along with replacement by HO^- is slightly less likely [calculated dissociation energy differences: −41 kcal mol^{-1} for μ_2(2-Er/Er), −24 kcal mol^{-1} for μ'_2(2-Er/Er), −54 kcal mol^{-1} for both ligands, Table S15 and Figure S48]. Removal of the μ_2(2-Er/Er) acetate ligand was accompanied by an additional water molecule entering the coordination sphere of Er^{3+} (Figure 8c). The absence of water association during MD simulation of the μ'_2(2-Er/Er) ligand dissociation is probably due to steric hindrance of the remaining μ_2(2-Er/Er) acetate by the neighboring hmp ligand blocking the way for incoming water molecules (Figure 8d). Nevertheless, detachment of the third μ_2(2-Co/Er) bridging acetate from either Co^{2+} or Er^{3+} (Figure 8b, Table S17 and Figure S50) is energetically plausible (energy differences −65 kcal mol^{-1} and −54 kcal mol^{-1}, respectively). In contrast, computational results indicate that dissociation of a monodentate $\mu(1)$ acetate ligand from **1** is less probable (Table S14 and Figures S46, cf. also Tables S19 and S20, Figures S45 and S54: smaller model within a static approach).

During the MD run of **1** with acetate in solution and hydroxide attached, a proton from an adjacent water molecule was transferred to that hydroxide forming a water ligand, which hydrogen-bonded the newly formed OH^- for the whole remaining duration of the MD trajectory. The transformation of a hydroxide ligand to a water ligand therefore appears to go over only a small barrier. Of the four investigated opening scenarios for the $\mu_2(1)$- and $\mu'_2(1)$-bidentate acetates (Figure 8e, Table S16 and Figure S49), partial dissociation of both "top" $\mu_2(1)$ and "bottom" $\mu'_2(1)$ bridging ligands is not favorable (30 kcal mol^{-1} and 18 kcal mol^{-1}, respectively). However, partial detachment of both bridging ligands from their substitution sites followed by attachment of water becomes far more likely (energy difference −2 kcal mol^{-1} and 1 kcal mol^{-1}, respectively) after replacement of one $\mu(1)$ ligand with HO^- (cf. background of Figure 8e). Therefore, the $\mu(1)$ monodentate acetate ligand represents an energetic bottleneck for the subsequent activation of both bidentate ligand sites of **1**. Notwithstanding methodological differences, both FT-IR monitoring and computational modeling approaches clearly point to superior ligand mobility of 2-Er over **1**. Interestingly, the WOC peak activities of 2-Er and 2-Ho (Figures 2, 7, S37 and Table S4) among the title compounds also coincide with highest water exchange rates of their respective Ln^{3+} centers among the series.[33] Moreover, the observed detrimental influence of phosphate buffer on the WOC activity (Table S3) is well in line with our calculations. Whereas mono- or bidentate chelation of borate buffer to **1** is unlikely (31 and 38 kcal mol^{-1}, respectively. cf. Table S18, Figures S51 and S52), bidentate bridging coordination of phosphate buffer ions is energetically more favorable (−6 kcal mol^{-1} compared to 44 kcal mol^{-1} for monodentate phosphate, cf. Table S18 and Figure S53). Our findings furthermore illustrate the significant impact of "spectator" anions and buffer media on the catalytic efficiency,[34] such as the observed inhibitory effect of deprotonated phosphate donor ligands on the active sites of potential dinuclear Co-WOCs.[35]

3. CONCLUSIONS

The $\{Co^{II}_3Ln(OR)_4\}$ ($[Co^{II}_3Ln(hmp)_4(OAc)_5H_2O]$, Ln = Ho - Yb) 2-Ln cubanes promote bioinspired design of water oxidation catalysts on new structural, analytical and computational/mechanistic levels.

(1) The $\{Co^{II}_3Ln(OR)_4\}$ cubanes are the first molecular 3d−4f catalysts for key photochemical processes with tunable Ln^{3+} centers. Consequently, four redox active centers are not mandatory to construct highly active cubane WOCs. The 2-Ln series with redox-inactive Ca^{2+} analogues in a mobile ligand environment newly translate OEC principles into active molecular WOCs. They compare favorably to bioinspired molecular cubanes in terms of maximum TON (211) and TOF values (9 s^{-1}).

(2) Stability of the $\{Co^{II}_3Ln(OR)_4\}$ cubanes under photochemical conditions was established in three stages: (a) spectroscopic solution tests and exclusion of nanoparticles, e.g., by DLS, (b) trace metal tests with Co^{2+} chelators (EDTA/Chelex resins) or ICP-MS analyses, and (c) postcatalytic structural integrity checks encompassing HPLC analyses as well as XANES/EXAFS spectroscopy.

(3) Next, photocatalytic and computational results based on innovative Ln-containing Born−Oppenheimer MD provide the proof-of-principle for Ln^{3+} centers as active catalytic promoters with flexible ligand binding modes in close analogy to OEC mechanisms.[15,24,36] A detailed investigation into subtle effects of the different Ln metal centers and the underlying mechanisms will be in the focus of further studies. Although the first step hole transfer rates for 2-Ln and the $\{Co^{II}_4(OR)_4\}$ reference cubane **1** correlate with their respective electrochemical driving forces, the superior $\{Co^{II}_3Ln(OR)_4\}$ WOC performance over **1** illustrates that rapid initial kinetics in the four-electron-transfer process do not necessarily result in higher overall O_2 yields. All in all, the $\{Co^{II}_3Ln(OR)_4\}$ cubanes are a new platform for evaluating the impact of bioinspired motifs on synthetic catalyst design.

■ ASSOCIATED CONTENT

Supporting Information

The Supporting Information is available free of charge on the ACS Publications website at DOI: 10.1021/jacs.5b05831.

Detailed synthetic, catalytic, analytical, and computational methods and results (PDF)

■ AUTHOR INFORMATION

Corresponding Authors

*sandra.luber@chem.uzh.ch

*greta.patzke@chem.uzh.ch

Notes

The authors declare no competing financial interest.

■ ACKNOWLEDGMENTS

Financial support by the Swiss National Science Foundation (Sinergia Grant No. CRSII2_136205/1) is gratefully acknowledged. The work has been supported by the University Research Priority Program (URPP) for solar light to chemical energy conversion (LightChEC). We thank the National Center of Competence in Research—Materials Revolution: Computational Design and Discovery of Novel Materials (NCCR-MARVEL) for financial support, and the Swiss National

DOI: 10.1021/jacs.5b05831
J. Am. Chem. Soc. 2015, 137, 11076−11084

Supercomputing Center (project ID: s502) for computing resources. Dr. Paula Abdala and Dr. Herman Emerich (ESRF Grenoble) are acknowledged for beamline support.

REFERENCES

(1) (a) Lewis, N. S.; Nocera, D. G. *Proc. Natl. Acad. Sci. U. S. A.* **2006**, *103*, 15729−15735. (b) Berardi, S.; Drouet, S.; Francàs, L.; Gimbert-Surinach, G.; Guttentag, M.; Richmond, C.; Stoll, T.; Llobet, A. *Chem. Soc. Rev.* **2014**, *43*, 7501−7519. (c) Alibabaei, L.; Brennaman, M. K.; Norris, M. R.; Kalanyan, B.; Song, W.; Losego, M. D.; Concepcion, J. J.; Binstead, R. A.; Parsons, G. N.; Meyer, T. J. *Proc. Natl. Acad. Sci. U. S. A.* **2013**, *110*, 20008−20013. (d) Styring, S. *Faraday Discuss.* **2012**, *155*, 357−376. (e) Tachibana, Y.; Vayssieres, L.; Durrant, J. *Nat. Photonics* **2012**, *6*, 511−518.

(2) (a) Young, K. J.; Martini, L. A.; Milot, R. L.; Snoeberger, R. C.; Batista, V. S.; Schmuttenmaer, C. A.; Crabtree, R. H.; Brudvig, G. W. *Coord. Chem. Rev.* **2012**, *256*, 2503−2520. (b) Sartorel, A.; Bonchio, M.; Campagna, S.; Scandola, F. *Chem. Soc. Rev.* **2013**, *42*, 2262−2280. (c) Barnett, S. M.; Goldberg, K. L.; Mayer, J. M. *Nat. Chem.* **2012**, *4*, 498−502. (d) McAlpin, J. G.; Stich, T. A.; Casey, W. H.; Britt, R. D. *Coord. Chem. Rev.* **2012**, *256*, 2445−2452. (e) Duan, L.; Bozoglian, F.; Mandal, S.; Stewart, B.; Privalov, T.; Llobet, A.; Sun, L. *Nat. Chem.* **2012**, *4*, 418−423. (f) Kärkäs, M. D.; Verho, O.; Johnston, E. V.; Åkermark, B. *Chem. Rev.* **2014**, *114*, 11863−12001. (g) Chen, H.-C.; Hetterscheid, D. G. H.; Williams, R. M.; van der Vlugt, J. I.; Reek, J. N. H.; Brouwer, A. M. *Energy Environ. Sci.* **2015**, *8*, 975−982. (h) Wang, L.; Mirmohades, M.; Brown, A.; Duan, L.; Li, F.; Daniel, Q.; Lomoth, R.; Sun, L.; Hammarström, L. *Inorg. Chem.* **2015**, *54*, 2742−2751. (i) Willkomm, J.; Muresan, N. M.; Reisner, E. *Chem. Sci.* **2015**, *6*, 2727−2736. (j) Najafpour, M. M.; Fekete, M.; Sedigh, D. J.; Aro, E.; Carpentier, R.; Eaton-Rye, J. J.; Nishihara, H.; Shen, J.-R.; Allakhverdiev, S. I.; Spiccia, L. *ACS Catal.* **2015**, *5*, 1499−1512.

(3) (a) Umena, Y.; Kawakami, K.; Shen, V.; Kamiya, N. *Nature* **2011**, *473*, 55−65. (b) Hutchings, G. S.; Zhang, Y.; Li, J.; Yonemoto, B. T.; Zhou, X. T.; Zhu, K.; Jiao, F. *J. Am. Chem. Soc.* **2015**, *137*, 4223−4229. (c) Liao, R.-Z.; Kärkäs, M. B.; Lee, B.-L.; Åkermark, B.; Siegbahn, P. E. M. *Inorg. Chem.* **2015**, *54*, 342−351. (d) Pichon, A. *Nat. Chem.* **2015**, *7*, 465−468. (e) Lang, S. M.; Fleischer, I.; Bernhardt, T. M.; Barnett, R. N.; Landman, U. *J. Phys. Chem. C* **2015**, *119*, 10881−10887. (f) Young, K. J.; Brennan, B. J.; Tagore, R.; Brudvig, G. W. *Acc. Chem. Res.* **2015**, *48*, 567−574.

(4) (a) Tsui, E.; Agapie, T. *Proc. Natl. Acad. Sci. U. S. A.* **2013**, *110*, 10084−10088. (b) Risch, M.; Ringleb, F.; Kohlhoff, M.; Bogdanoff, P.; Chernev, P.; Zaharieva, I.; Dau, H. *Energy Environ. Sci.* **2015**, *8*, 661−674.

(5) (a) Smith, P. F.; Kaplan, C.; Sheats, J. E.; Robinson, D. M.; McCool, N. S.; Mezle, N.; Dismukes, G. C. *Inorg. Chem.* **2014**, *53*, 2113−2121. (b) Ullman, A. M.; Liu, Y.; Huynh, M.; Bediako, D. K.; Wang, H.; Anderson, B. L.; Powers, D. C.; Breen, J. J.; Abruna, H. D.; Nocera, D. G. *J. Am. Chem. Soc.* **2014**, *136*, 17681−17688. (c) Genoni, A.; La Ganga, G.; Volpe, A.; Puntoriero, F.; Di Valentin, M.; Bonchio, M.; Natali, M.; Sartorel, A. *Faraday Discuss.* **2015**, DOI: 10.1039/C5FD00076A.

(6) Zhang, C.; Trudel, S.; Berlinguette, C. P. *Eur. J. Inorg. Chem.* **2014**, *2014*, 660−664.

(7) (a) Galán-Máscaros, J. R. *ChemElectroChem* **2015**, *2*, 37−50. (b) Jiao, Y.; Zheng, Y.; Jaroniec, M.; Qiao, S. Z. *Chem. Soc. Rev.* **2015**, *44*, 2060−2074. (c) Han, X.-B.; Zhang, Z.-M.; Zhang, T.; Li, Y.-G.; Lin, W.; You, W.; Su, Z.-M.; Wang, E.-B. *J. Am. Chem. Soc.* **2014**, *136*, 5359−5366. (d) Han, X. B.; Li, Y.-G.; Zhang, Z.-M.; Tan, H.-Q.; Lu, Y.; Wang, E.-B. *J. Am. Chem. Soc.* **2015**, *137*, 5486−5493.

(8) (a) Artero, V.; Chavarot-Kerlidou, M.; Fontecave, M. *Angew. Chem., Int. Ed.* **2011**, *50*, 7238−7266. (b) Stracke, J. J.; Finke, R. G. *ACS Catal.* **2014**, *4*, 909−933. (c) Lv, H.; Song, J.; Geletii, Y. V.; Vickers, J. W.; Sumliner, J. M.; Musaev, D. G.; Kögerler, P.; Zhuk, P. F.; Bacsa, J.; Zhu, G.; Hill, C. L. *J. Am. Chem. Soc.* **2014**, *136*, 9268−9271. (d) Li, X.; Siegbahn, P. E. M. *J. Am. Chem. Soc.* **2013**, *135*, 13804−13813. (e) Sala, X.; Maji, S.; Bofill, R.; García-Antón, J.; Escriche, L.; Llobet, A. *Acc. Chem. Res.* **2014**, *47*, 504−516. (f) Hijazi, A.; Kemmegne-Mbouguen, J. G.; Floquet, S.; Marrot, J.; Mayer, C. R.; Artero, V.; Cadot, E. *Inorg. Chem.* **2011**, *50*, 9031−9038. (g) Artero, V.; Fontecave, M. *Chem. Soc. Rev.* **2013**, *42*, 2338−2356. (h) Zhang, M.; de Respinis, M.; Frei, H. *Nat. Chem.* **2014**, *6*, 362−367. (i) Yamada, Y.; Oyama, K.; Gates, R.; Fukuzumi, S. *Angew. Chem., Int. Ed.* **2015**, *54*, 5613−5617.

(9) (a) Bang, S.; Lee, Y. M.; Hong, S.; Cho, K. B.; Nishida, Y.; Seo, M. S.; Sarangi, R.; Fukuzumi, S.; Nam, S. *Nat. Chem.* **2014**, *6*, 934−940. (b) Cox, N.; Rapatskiy, L.; Su, J.-H.; Pantazis, D. A.; Sugiura, M.; Kulik, L.; Dorlet, P.; Rutherford, A. W.; Neese, F.; Boussac, A.; Lubitz, W.; Messinger, J. *J. Am. Chem. Soc.* **2011**, *133*, 3635−3648.

(10) (a) McCool, N. S.; Robinson, D. M.; Sheats, J. E.; Dismukes, G. C. *J. Am. Chem. Soc.* **2011**, *133*, 11446−11449. (b) Berardi, S.; La Ganga, G.; Natali, M.; Bazzan, I.; Puntoriero, P.; Sartorel, A.; Scandola, F.; Campagna, S.; Bonchio, M. *J. Am. Chem. Soc.* **2012**, *134*, 11104−11107. (c) Zhang, B.; Li, F.; Yu, F.; Wang, X.; Zhou, X.; Li, H.; Jiang, Y.; Sun, L. *ACS Catal.* **2014**, *4*, 804−809. (d) Evangelisti, F.; Güttinger, R.; Moré, R.; Luber, S.; Patzke, G. R. *J. Am. Chem. Soc.* **2013**, *135*, 18734−18737.

(11) Al-Oweini, R.; Sartorel, A.; Bassil, B. S.; Natali, M.; Berardi, S.; Scandola, F.; Kortz, U.; Bonchio, M. *Angew. Chem., Int. Ed.* **2014**, *53*, 11182−11185.

(12) (a) Lin, P.-H.; Takase, M. K.; Agapie, T. *Inorg. Chem.* **2015**, *54*, 59−64. (b) Mukherjee, S.; Stull, J. A.; Yano, J.; Stamatatos, T. C.; Pringouri, K.; Stich, T. A.; Abboud, K. A.; Britt, R. D.; Yachandra, V. K.; Christou, G. *Proc. Natl. Acad. Sci. U. S. A.* **2012**, *109*, 2257−2262. (c) Hocking, R. K.; Brimblecombe, R. L.; Chang, Y.; Singh, A.; Cheah, M. H.; Glover, C.; Casey, W. H.; Spiccia, L. *Nat. Chem.* **2011**, *3*, 461−466. (d) Kanady, J. S.; Tsui, E. Y.; Day, M. W.; Agapie, T. *Science* **2011**, *333*, 733−736.

(13) Zhang, C.; Chen, C.; Dong, H.; Shen, J. R.; Dau, H.; Zhao, J. *Science* **2015**, *348*, 690−693.

(14) Hibberd, A. H.; Doan, H. Q.; Glass, E. N.; de Groot, F. M. F.; Hill, C. L.; Cuk, T. K. *J. Phys. Chem. C* **2015**, *119*, 4173−4179.

(15) Service, R. J.; Yano, J.; McConnell, I.; Hwang, H. J.; Niks, D.; Hille, R.; Wydrzynski, T.; Burnap, R. L.; Hillier, W.; Debus, R. J. *Biochemistry* **2011**, *50*, 63−81.

(16) Wang, P.; Shannigrahi, S.; Yakovlev, N. L.; Hor, T. S. *Inorg. Chem.* **2012**, *51*, 12059−12061.

(17) Pizzolato, E.; Natali, M.; Posocco, B.; López, A.; Bazzan, I.; Di Valentin, M.; Galloni, P.; Conte, V.; Bonchio, M.; Scandola, F.; Sartorel, A. *Chem. Commun.* **2013**, *49*, 9941−9943.

(18) Wasylenko, D. J.; Palmer, R. D.; Berlinguette, C. *Chem. Commun.* **2013**, *49*, 218−227.

(19) Goberna-Ferrón, S.; Vigara, L.; Soriano-López, J.; Galán-Máscaros, J. *Inorg. Chem.* **2012**, *51*, 11707−11715.

(20) Huang, Z.; Luo, Z.; Geletii, Y. V.; Vickers, J. W.; Yin, Q.; Wu, D.; Hou, Y.; Ding, Y.; Song, J.; Musaev, D. G.; Hill, C. L.; Lian, T. *J. Am. Chem. Soc.* **2011**, *133*, 2068−2072.

(21) Kanan, M. W.; Surendranath, Y.; Nocera, D. G. *Chem. Soc. Rev.* **2009**, *38*, 109−114.

(22) Mattioli, G.; Giannozzi, P.; Bonapasta, A. A.; Guidoni, L. *J. Am. Chem. Soc.* **2013**, *135*, 15353−15363.

(23) Wang, L.-P.; Van Voorhis, T. *J. Phys. Chem. Lett.* **2011**, *2*, 2200−2204.

(24) (a) Bakou, A.; Buser, C.; Dandulakis, G.; Brudvig, G.; Ghanotakis, D. F. *Biochim. Biophys. Acta, Bioenerg.* **1992**, *1099*, 131−136. (b) Bakou, A.; Ghanotakis, D. F. *Biochim. Biophys. Acta, Bioenerg.* **1993**, *1141*, 303−308. (c) Lee, C. I.; Lakshmi, K. V.; Brudvig, G. W. *Biochemistry* **2007**, *46*, 3211−3223.

(25) Evangelisti, F.; Car, P.-E-; Blacque, O.; Patzke, G. R. *Catal. Sci. Technol.* **2013**, *3*, 3117−3129.

(26) Wang, D.; Groves, J. T. *Proc. Natl. Acad. Sci. U. S. A.* **2013**, *110*, 15579−15584.

(27) Vickers, J. W.; Lv, H.; Sumliner, J. M.; Zhu, G.; Luo, Z.; Musaev, D. G.; Geletii, Y. V. *J. Am. Chem. Soc.* **2013**, *135*, 14110−14118.

(28) McCrory, C. C. L; Jung, S.; Ferrer, I. M.; Chatman, S. M.; Peters, J. C.; Jaramillo, T. F. *J. Am. Chem. Soc.* **2015**, *137*, 4347−4357.

(29) Eilers, G.; Zettersten, C.; Nyholm, L.; Hammarström, L.; Lomoth, R. *Dalton Trans.* **2005**, 1033−1041.

DOI: 10.1021/jacs.5b05831
J. Am. Chem. Soc. 2015, 137, 11076−11084

(30) McNamara, W. R.; Han, Z.; Yin, C.-J.; Brennessel, W. W.; Holland, P. L.; Eisenberg, R. *Proc. Natl. Acad. Sci. U. S. A.* **2012**, *109*, 15594−15599.
(31) Thomsen, J. M.; Sheehan, S. W.; Hashmi, S. M.; Campos, J.; Hintermair, U.; Crabtree, R. H.; Brudvig, G. W. *J. Am. Chem. Soc.* **2014**, *136*, 13826−13834.
(32) Klamt, A.; Schüürmann, G. *J. Chem. Soc., Perkin Trans. 2* **1993**, *2*, 799−805.
(33) D'Angelo, P.; Spezia, R. *Chem. - Eur. J.* **2012**, *18*, 11162−11178.
(34) Vannucci, A. K.; Alibabaei, L.; Losego, M. D.; Concepcion, J. J.; Kalanyan, B.; Parsons, G. N.; Meyer, T. J. *Proc. Natl. Acad. Sci. U. S. A.* **2013**, *110*, 20918−20922.
(35) Davenport, T. C.; Ahn, H. S.; Ziegler, M. S.; Tilley, T. D. *Chem. Commun.* **2014**, *50*, 6326−6329.
(36) Pal, R.; Negre, C. F. A.; Vogt, L.; Pokhrel, R.; Ertem, M. Z.; Brudvig, G. W.; Batista, V. S. *Biochemistry* **2013**, *52*, 7703−7706.

DOI: 10.1021/jacs.5b05831
J. Am. Chem. Soc. 2015, 137, 11076−11084